PERGAMON

International Journal of Solids and Structures 38 (2001) 4857–4878

INTERNATIONAL JOURNAL OF SOLIDS and STRUCTURES

www.elsevier.com/locate/ijsolstr

# Three-dimensional thermoelastic wave motions in a half-space under the action of a buried source

G. Lykotrafitis [a], H.G. Georgiadis [a,*], L.M. Brock [b]

[a] *Mechanics Division, National Technical University of Athens, 5 Heroes of Polytechnion Avenue, Zographou GR-15773, Greece*
[b] *Department of Mechanical Engineering, University of Kentucky, 521 CRMS Building, Lexington, KY 40506-0108, USA*

Received 28 December 1999; in revised form 20 July 2000

**Abstract**

A three-dimensional (3D) transient dynamic problem within Biot's coupled thermoelastic theory is studied in this paper. It involves a half-space acted upon by a thermal and mechanical buried point source. It is assumed that the half-space behaves like a coupled thermoelastic solid, whereas the loading consists of a concentrated heat flux (thermal source) and a concentrated force (mechanical source) of arbitrary direction with respect to the half-space surface. Both thermal and mechanical sources are situated at the same point in the interior of the half-space. The problem aims at modeling both underground explosions and impulsively applied heat loadings near a boundary. In addition, the present solution provides the necessary Green's function which can be employed in the boundary element method for numerical treatment of more complicated transient thermoelastodynamic problems involving half-space geometries (e.g. domains with openings or contact problems). The situation studied here is the 3D analogue of a recent plane-strain problem considered by Georgiadis et al. (1999a). It can also be viewed as a generalization of the classical buried-force elastodynamic problem of Pekeris (1955) in the sense that more complicated material behavior and loading are considered. The associated initial/boundary value problem is treated via unilateral and double bilateral Laplace transforms, which suppress, respectively, the time variable and two of the space variables. A $12 \times 12$ system of linear equations arises in the multiple transform domain and its exact solution is obtained by employing MATHEMATICA™. From this solution, results for the vertical displacement at the surface due to a buried thermal source are obtained through numerical wave number integrations and numerical unilateral Laplace-transform inversions. 

*Keywords:* Thermoelasticity; Waves; Three-dimensional problems; Green's functions

## 1. Introduction

The present work is a sequel of a recent study by Georgiadis et al. (1999a) considering the transient thermoelastodynamic disturbances produced in a linear coupled thermoelastic half-plane under the action of a buried *line* thermal/mechanical source (plane-strain problem). Here, the corresponding

* Corresponding author. Tel.: +30-1-772-1365; fax: +30-1-772-1302.
*E-mail address:* georgiad@central.ntua.gr (H.G. Georgiadis).

0020-7683/01/$ - see front matter 
PII: S0020-7683(00)00311-5

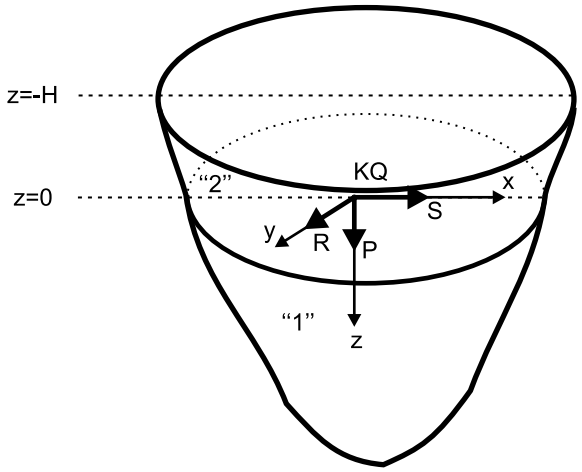


Fig. 1. 3-D thermoelastic half-space under the action of buried thermal and mechanical point sources.

three-dimensional (3D) problem is treated. The thermal point-source is a concentrated heat flux and the mechanical point-source is a force with different horizontal and vertical components (Fig. 1). Both sources are situated at the same location in a fixed distance from the surface of the half-space and may have an arbitrary time dependence. The present problem and its plane-strain version studied earlier (Georgiadis et al. 1999a) have relevance to: (i) the case of underground nuclear explosions (Bullen and Bolt, 1987), (ii) the case of sudden heat radiation due to accidents involving nuclear waste buried in the ground, (iii) the case of sudden heat loadings by impulsive electromagnetic radiation (Morland, 1968; Hegemier and Tzung, 1970; Sve and Miklowitz, 1973; Bechtel, 1975; Hetnarski and Ignaczak, 1994; Hata, 1995), and (iv) the boundary element method as fundamental solutions (see corresponding formulations and problems in thermoelastic full spaces Predeleanu, 1987; Fleurier and Predeleanu, 1987; Sharp and Crouch, 1987; Manolis and Beskos, 1989, 1990; Wang and Dhaliwal, 1993).

It should be noted, however, that the previous studies concerning sudden heat loadings model the problem as a *one-dimensional* or employ *uncoupled* thermoelasticity. Also, the studies concerning fundamental solutions treat only *infinite* domains (i.e. full spaces) and often consider *time-harmonic* response. On the contrary, the present study aims at a more realistic formulation of these problems and is therefore based on the transient coupled thermoelastodynamic theory, while it treats a 3D problem in a half-space domain.

Regarding the relevance of the constitutive theory (Biot, 1956; Chadwick, 1960; Carlson, 1972) to the present problem, we notice that in *thermal-shock* problems, the importance of inertia (dynamic) effects was revealed in the studies of Sternberg and Chakravorty (1959a,b) and the importance of both inertia and thermal-coupling effects in the studies of Hetnarski (1961), Boley and Tolins (1962), and Francis (1972).

Now, the problem of a buried mechanical source in an elastic half-plane or half-space (no thermal effects) has a long and interesting history for the areas of wave propagation and Geodynamics. Important contributions were made by Pekeris (1955), Garvin (1956), Pekeris and Lifson (1957), Aggarwal and Ablow (1967), Payton (1968, 1983), Johnson (1974), and Tsai and Ma (1991). This problem, apart from other applications, can be used in modeling earthquake activity (Burridge and Knopoff, 1964).

In the present study, we deal with a related but more general problem than those of Pekeris and Johnson since a more complex constitutive theory (Biot's theory) than classical elasticity is employed and thermal loading is considered as well. Within the same context (i.e. transient coupled thermoelastodynamics), recent efforts dealing with *crack* and *moving load* problems are due to Atkinson and Craster (1992), Chen and Kuo (1994), Brock (1995, 1997), Brock et al. (1996, 1997), and Georgiadis et al. (1998), among others. In our

work, the resulting system of coupled hyperbolic and parabolic PDEs and the pertinent initial and boundary conditions are attacked with unilateral and multiple bilateral Laplace transforms. To deal with the source terms without considering them in the field equations, we follow a procedure introduced by Pekeris (1955) and also employed by Payton (1983), Vardoulakis and Harnpattanapanich (1986), and Georgiadis et al. (1999a). This procedure separates the half-space into two regions (a half-space region extending below the horizontal source plane and a strip-like region extending between the source plane and the surface plane of the original half-space) with different representations of multiple transformed displacements, stresses and temperature. Then, the exact transformed solution is obtained by considering the appropriate continuity and discontinuity conditions along the source plane. The resulting $12 \times 12$ system of linear equations has also to be solved exactly (in symbolic form) in the multiple transform domain, and this was made possible through the use of MATHEMATICA™. Explicit numerical results for the vertical surface displacement are given here in the case of a thermal loading. The numerical problem of *transform inversions* is particularly challenging since integrals of rapidly oscillatory functions over semi-infinite interval (wave number integrals – see e.g. Xu and Mal (1985), Mal and Lih (1992) and Lih and Mal (1992)) are involved along with unilateral Laplace-transform inversion. To deal with this, a strategy similar to the one in Georgiadis et al. (1999a) was followed. More specifically, for the oscillatory integrands, which in addition may take very large values (pseudo-pole behavior) at certain points, we follow the concept of Longman's (1956) method but using as accelerator in the summation procedure a modified epsilon algorithm instead of the standard Euler's transformation. Also, an adaptive procedure using the Gauss 80-point rule is employed to integrate in the vicinity of the pseudo-pole. The numerical Laplace-transform inversion is carried out through the robust Fourier-series technique of Crump (1976).

## 2. Problem statement

Consider a 3D body in the form of a half-space $z > -H$ (Fig. 1) governed by coupled thermoelasticity. The body is initially at rest and at uniform temperature. At time $t = 0$, thermal and mechanical sources both start acting at the point $(x = 0, y = 0, z = 0)$, which is taken as the origin of the Cartesian coordinate system $xyz$ and is situated at a depth $H$ below the surface. The concentrated thermal loading has a time dependence $g_Q(t)$ and an intensity $KQ$, where $K$ is the thermal conductivity with dimensions of (power) (unit length)$^{-1}$ (°C)$^{-1}$, °C means degrees of temperature and $Q$ is a multiplier expressed in (°C) (unit length) (dimensions of $g_Q(t)$)$^{-1}$. The concentrated mechanical loading has a vertical component $Pg_P(t)$, and horizontal components $Sg_S(t)$ and $Rg_R(t)$, where $g_P(t)$, $g_S(t)$ and $g_R(t)$ denote time dependencies. Here, the intensities $P$, $S$ and $R$ are expressed in (force) (dimensions of $g_j(t)$)$^{-1}$, with $(j = P, S, R)$. Finally, all time dependencies $g_k(t)$, with $(k = Q, P, S, R)$, may be arbitrary functions but of bounded variation as $t \to \infty$; the latter being an assumption which secures that these functions are amenable to unilateral Laplace transformation. Then, according to the linear isotropic coupled thermoelastodynamic theory of Biot (1956) (see also e.g. Carlson, 1972), the governing equations for this problem are written as

$$\boldsymbol{\sigma} = \mu(\nabla \boldsymbol{u} + \boldsymbol{u}\nabla) + \lambda(\nabla \cdot \boldsymbol{u})\mathbf{1} - \kappa_0(3\lambda + 2\mu)\theta\mathbf{1}, \tag{1}$$

$$\boldsymbol{q} = -K\nabla\theta, \tag{2}$$

$$\mu\nabla^2\boldsymbol{u} + (\lambda + \mu)\nabla(\nabla \cdot \boldsymbol{u}) - \kappa_0(3\lambda + 2\mu)\nabla\theta + \boldsymbol{f}\delta(x)\delta(y)\delta(z) = \rho\frac{\partial^2\boldsymbol{u}}{\partial t^2}, \tag{3}$$

$$K\nabla^2\theta - \rho c_v\frac{\partial\theta}{\partial t} - \kappa_0(3\lambda + 2\mu)\tilde{T}_0\frac{\partial(\nabla \cdot \boldsymbol{u})}{\partial t} + KQg_Q(t)\,\delta(x)\,\delta(y)\,\delta(z) = 0, \tag{4}$$

where Eq. (1) is the Neumann–Duhamel relation, Eq. (2) is the heat conduction equation, Eq. (3) is the displacement–temperature equation of motion, and Eq. (4) is the coupled heat equation. Also, in the above equations, $\boldsymbol{\sigma}$ is the stress tensor; $\boldsymbol{u}$, the displacement vector; $\theta = \tilde{T} - \tilde{T}_0$, the change in temperature; $\tilde{T}$, the current temperature; $\tilde{T}_0$, the initial temperature; $\boldsymbol{q}$, the heat–flux vector whose components have dimensions of (power) (unit area)$^{-1}$; ($\lambda$ and $\mu$), the Lame constants; $\kappa_0$, the coefficient of linear expansion expressed in (°C)$^{-1}$; $\rho$, the mass density; $c_v$, the specific heat at constant deformation expressed in (energy) (unit mass)$^{-1}$ (°C)$^{-1}$; $\boldsymbol{f}$, a vector having $Sg_S(t)$ as its $x$-component, $Rg_R(t)$ as its $y$-component and $Pg_P(t)$ as its $z$-component; $\delta(\ )$ denotes the Dirac delta distribution with dimensions $(\ )^{-1}$; $\mathbf{1}$, the identity tensor; $\nabla$, the gradient operator; and $\nabla^2 = (\partial^2/\partial x^2) + (\partial^2/\partial y^2) + (\partial^2/\partial z^2)$ is the Laplace operator. All field quantities above are functions of $(x, y, z, t)$.

In addition, zero initial conditions are taken, i.e.

$$\boldsymbol{u} = \partial \boldsymbol{u}/\partial t = \theta = 0 \quad \text{for } t \leqslant 0 \quad \text{in } (-\infty < x < \infty,\ -\infty < y < \infty,\ -H < z < \infty), \tag{5}$$

and we also assume that the half-space surface $z = -H$ is traction free and insulated (i.e. no heat is conducted through the half-space surface and air). Finally, the pertinent *finiteness* conditions at remote regions (Ignaczak and Nowacki, 1962) state that the field at infinity remains bounded although temperature signals travel – according to Biot's theory – at an *infinite* speed,

Next, by following the method of Pekeris (1955), we introduce an imaginary plane along $(z = 0)$ separating the *original* half-space into the half-space $(0 < z < \infty)$ (region 1 in Fig. 1) and the strip $(-H < z < 0)$ (region 2 in Fig. 1), and consider pertinent continuity and discontinuity conditions at $z = 0$ along with the standard boundary conditions at $z = -H$:

$$u_{x1}(x, y, 0, t) = u_{x2}(x, y, 0, t), \tag{6a}$$

$$u_{y1}(x, y, 0, t) = u_{y2}(x, y, 0, t), \tag{6b}$$

$$u_{z1}(x, y, 0, t) = u_{z2}(x, y, 0, t), \tag{6c}$$

$$\theta_1(x, y, 0, t) = \theta_2(x, y, 0, t), \tag{6d}$$

$$\sigma_{zz1}(x, y, 0, t) - \sigma_{zz2}(x, y, 0, t) = Pg_P(t)\delta(x)\delta(y), \tag{6e}$$

$$\sigma_{zx1}(x, y, 0, t) - \sigma_{zx2}(x, y, 0, t) = Sg_S(t)\delta(x)\delta(y), \tag{6f}$$

$$\sigma_{zy1}(x, y, 0, t) - \sigma_{zy2}(x, y, 0, t) = Rg_R(t)\delta(x)\delta(y), \tag{6g}$$

$$\frac{\partial \theta_1(x, y, 0, t)}{\partial z} - \frac{\partial \theta_2(x, y, 0, t)}{\partial z} = Qg_Q(t)\delta(x)\delta(y), \tag{6h}$$

$$\sigma_{zz}(x, y, -H, t) = \sigma_{zx}(x, y, -H, t) = \sigma_{zy}(x, y, -H, t) = 0, \tag{7a}$$

$$\frac{\partial \theta(x, y, -H, t)}{\partial z} = 0, \tag{7b}$$

where $-\infty < x < \infty$, $-\infty < y < \infty$, and the subscript 1 or 2 in a field quantity means that the plane $z = 0$ is approached as $z \to 0^+$ or $z \to 0^-$, respectively. It is apparent now that introducing Eq. (6) allows to formulate the initial/boundary value problem without the explicit consideration of the *source* terms $\boldsymbol{f}\delta(x)\delta(y)\delta(z)$ and $KQg_Q(t)\delta(x)\delta(y)\delta(z)$ in the field Eqs. (3) and (4), respectively, and therefore, leads to a considerable reduction of algebraic manipulations.

In this way, the original problem (1)–(5) and (7a) and (7b) can alternatively be described by Eqs. (1), (2), (5)–(7a) and (7b) along with the following field equations (the latter being with no source terms):

$$\nabla^2 \boldsymbol{u} + \left(m^2 - 1\right)\nabla \Delta + \kappa \nabla \theta - m^2 \frac{\partial^2 \boldsymbol{u}}{\partial s^2} = 0, \tag{8}$$

$$\frac{\kappa}{m^2}\nabla^2 \theta - \frac{\kappa}{h m^2}\frac{\partial \theta}{\partial s} + \frac{\varepsilon}{h}\frac{\partial \Delta}{\partial s} = 0, \tag{9}$$

where Eqs. (8) and (9) follow directly from Eqs. (3) and (4) by introducing the shear-wave velocity $V_2 = (\mu/\rho)^{1/2}$, the dilatation $\Delta = \nabla \cdot \boldsymbol{u}$, the normalized time $s = V_1 t$, the normalized coefficient of linear expansion $\kappa = -\kappa_0(3\lambda + 2\mu)/\mu = \kappa_0(4 - 3m^2) < 0$, the dimensionless coupling coefficient $\varepsilon = (\tilde{T}_0/c_v)(\kappa V_2/m)^2$, and the thermoelastic characteristic length $h = (KV_2/\mu m c_v)$. Here, we also define $m = V_1/V_2 > 1$ and $V_1 = [(\lambda + 2\mu)/\rho]^{1/2}$, and it is of notice that the quantity $V_1$ is the longitudinal wave velocity in the absence of thermal effects (i.e. in the purely elastic theory). As regards the range of numerical values for the coupling coefficient and the thermoelastic length measured in several engineering materials, generally these are of the orders $\varepsilon = \mathrm{O}(10^{-2})$ and $h = \mathrm{O}(10^{-10})$ m (Chadwick, 1960).

Finally, for convenience in the subsequent analysis, the largely arbitrary functions of time dependence of the sources $g_k(t)$, with $(k = Q, P, S, R)$, are replaced by the Dirac $\delta(t)$ and, therefore, any response due to a general time dependence of the loading is obtainable from the present solution through *convolution*. Moreover, when the double transformed solution corresponding to the $\delta(t)$ loading is found below, we shall identify the pertinent alterations needed to provide the solution due to an arbitrary $g_k(t)$ loading.

## 3. Integral-transform analysis

The dependence of the problem on the variables $(x, y, s)$ is suppressed through the use of multiple Laplace transforms. The unilateral transform is defined as

$$\Phi(x, y, z, p) = \int_0^\infty \varphi(x, y, z, s)\mathrm{e}^{-ps}\,\mathrm{d}s, \tag{10a}$$

$$\varphi(x, y, z, s) = (1/2\pi\mathrm{i})\int_{\Gamma_1} \Phi(x, y, z, p)\mathrm{e}^{ps}\,\mathrm{d}p, \tag{10b}$$

whereas the double bilateral transform as

$$\Phi^*(q, w, z, p) = \int_{-\infty}^\infty \int_{-\infty}^\infty \Phi(x, y, z, p)\mathrm{e}^{-p(qx+wy)}\,\mathrm{d}x\,\mathrm{d}y, \tag{11a}$$

$$\Phi(x, y, z, p) = (p/2\pi\mathrm{i})^2 \int_{\Gamma_2}\int_{\Gamma_3} \Phi^*(q, w, z, p)\mathrm{e}^{p(qx+wy)}\,\mathrm{d}q\,\mathrm{d}w, \tag{11b}$$

where for the unilateral direct transform, we save a capital letter and the double bilateral direct transform is denoted by an asterisk. We also notice that (van der Pol and Bremmer, 1950): (1) Because of the identity theorem for analytic functions, it is sufficient to view $\Phi(x, y, z, p)$ as a function of a *real* variable $p$ over some segment of the real axis in the half-plane of analyticity. Once $\Phi(x, y, z, p)$ is determined as an explicit function of $p$ in the course of solving the transformed differential equations, its definition can be extended to the whole complex $p$-plane, except for isolated singular points, through analytic continuation. (2) The variables $q$ and $w$ are *complex*. (3) The integration path $\Gamma_j$, with $(j = 1, 2, 3)$, is a line parallel to the imaginary axis in the associated transform plane and lies *within* the region of analyticity.

Applying now Eqs. (10a) and (11a) to the governing equations (1), (8) and (9), and considering Eq. (5) yields the following general expressions for the transformed temperature change, displacements and stresses (some details of the procedure are given in Appendix A). These representations are, of course, different in regions 1 and 2.

*(a) Region 1 ($0 < z < \infty$):*

$$\begin{bmatrix} \frac{\kappa}{m^2}\Theta^* \\ pU_x^* \\ pU_y^* \\ pU_z^* \\ \frac{1}{\mu}\Sigma_{xy}^* \\ \frac{1}{\mu}\Sigma_{xz}^* \\ \frac{1}{\mu}\Sigma_{yz}^* \\ \frac{1}{\mu}\Sigma_{xx}^* \\ \frac{1}{\mu}\Sigma_{yy}^* \\ \frac{1}{\mu}\Sigma_{zz}^* \end{bmatrix} = \begin{bmatrix} M_+ & M_- & 0 & 0 & 0 & 0 & 0 & 0 \\ -q & -q & 1 & 0 & 0 & 0 & 0 & 0 \\ -w & -w & 0 & 1 & 0 & 0 & 0 & 0 \\ a_+ & a_- & \frac{q}{\beta} & \frac{w}{\beta} & 0 & 0 & 0 & 0 \\ -2qw & -2qw & w & q & 0 & 0 & 0 & 0 \\ 2qa_+ & 2qa_- & -\frac{T_w}{\beta} & \frac{wq}{\beta} & 0 & 0 & 0 & 0 \\ 2wa_+ & 2wa_- & \frac{wq}{\beta} & -\frac{T_q}{\beta} & 0 & 0 & 0 & 0 \\ T_{w^+} & T_{w^-} & 2q & 0 & 0 & 0 & 0 & 0 \\ T_{q^+} & T_{q^-} & 0 & 2w & 0 & 0 & 0 & 0 \\ -T & -T & -2q & -2w & 0 & 0 & 0 & 0 \end{bmatrix} \begin{bmatrix} X_1 e^{-pa_+ z} \\ X_2 e^{-pa_- z} \\ X_3 e^{-p\beta z} \\ X_4 e^{-p\beta z} \\ 0 \\ 0 \\ 0 \\ 0 \end{bmatrix}, \tag{12}$$

*(b) Region 2 ($-H < z < 0$):*

$$\begin{bmatrix} \frac{\kappa}{m^2}\Theta^* \\ pU_x^* \\ pU_y^* \\ pU_z^* \\ \frac{1}{\mu}\Sigma_{xy}^* \\ \frac{1}{\mu}\Sigma_{xz}^* \\ \frac{1}{\mu}\Sigma_{yz}^* \\ \frac{1}{\mu}\Sigma_{xx}^* \\ \frac{1}{\mu}\Sigma_{yy}^* \\ \frac{1}{\mu}\Sigma_{zz}^* \end{bmatrix} = \begin{bmatrix} M_+ & M_+ & M_- & M_- & 0 & 0 & 0 & 0 \\ -q & -q & -q & -q & 1 & 0 & 1 & 0 \\ -w & -w & -w & -w & 0 & 1 & 0 & 1 \\ -a_+ & a_+ & -a_- & a_- & \frac{-q}{\beta} & \frac{-w}{\beta} & \frac{q}{\beta} & \frac{w}{\beta} \\ -2qw & -2qw & -2qw & -2qw & w & q & w & q \\ -2qa_+ & 2qa_+ & -2qa_- & 2qa_- & \frac{T_w}{\beta} & \frac{-wq}{\beta} & \frac{-T_w}{\beta} & \frac{wq}{\beta} \\ -2wa_+ & 2wa_+ & -2wa_- & 2wa_- & \frac{-wq}{\beta} & \frac{T_q}{\beta} & \frac{wq}{\beta} & \frac{-T_q}{\beta} \\ T_{w^+} & T_{w^+} & T_{w^-} & T_{w^-} & 2q & 0 & 2q & 0 \\ T_{q^+} & T_{q^+} & T_{q^-} & T_{q^-} & 0 & 2w & 0 & 2w \\ -T & -T & -T & -T & -2q & -2w & -2q & -2w \end{bmatrix} \begin{bmatrix} X_5 e^{pa_+ z} \\ X_6 e^{-pa_+ z} \\ X_7 e^{p\alpha_- z} \\ X_8 e^{-p\alpha_- z} \\ X_9 e^{p\beta z} \\ X_{10} e^{p\beta z} \\ X_{11} e^{-p\beta z} \\ X_{12} e^{-p\beta z} \end{bmatrix}, \tag{13}$$

where $(U_x^*, U_y^*, U_z^*)$ and $(\Sigma_{xy}^*, \Sigma_{xz}^*, \ldots, \Sigma_{zz}^*)$ are the multiply transformed components of, respectively, the displacement vector and the stress tensor. We should also notice that solution (12) is bounded at $z \to \infty$ appropriately satisfying thus the finiteness conditions, whereas such constraints need not be imposed on solution (13). In the above equations, the yet unknown $X_1, X_2, \ldots, X_{12}$ are arbitrary functions of $(q, w, p)$ which will be determined from conditions (6a)–(6h) and (7a) and (7b) in our particular problem. The representation (12) is identical with Eq. (54) in Brock et al. (1996) but Eq. (13) appears for the first time. Also, the following definitions were employed:

$$\alpha_\pm = \left(m_\pm^2 - q^2 - w^2\right)^{1/2}, \qquad \beta = \left(m^2 - q^2 - w^2\right)^{1/2}, \tag{14a, b}$$

$$m_\pm = \frac{1}{2}\left[\left(1 + \frac{1}{(hp)^{1/2}}\right)^2 + \frac{\varepsilon}{hp}\right]^{1/2} \pm \frac{1}{2}\left[\left(1 - \frac{1}{(hp)^{1/2}}\right)^2 + \frac{\varepsilon}{hp}\right]^{1/2}, \tag{15}$$

$$M_\pm = m_\pm^2 - 1, \tag{16}$$

$$T = 2\beta^2 - m^2 = m^2 - 2(q^2 + w^2), \qquad T_\pm = 2a_\pm^2 - m^2, \tag{17a, b}$$

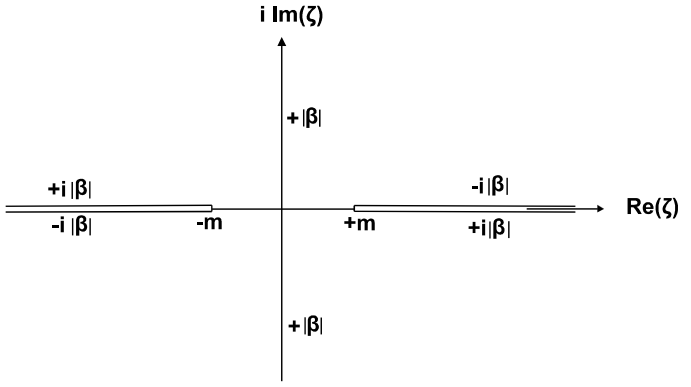


Fig. 2. The cut complex $\zeta$-plane for the function $\beta(\zeta) = \left(m^2 - \zeta^2\right)^{1/2}$. Similar branch cuts, emanating from the points $m_{\pm}(p)$, are also introduced to render the functions $a_{\pm}(\zeta) = \left(m_{\pm}^2 - \zeta^2\right)^{1/2}$ single valued.

$$T_{q\pm} = T_{\pm} + 2q^2, \qquad T_{w\pm} = T_{\pm} + 2w^2, \tag{18a, b}$$

$$T_q = T + q^2, \qquad T_w = T + w^2. \tag{19a, b}$$

Further, a new complex variable $\zeta$ is defined through $\zeta^2 = q^2 + w^2$, allowing the introduction of pertinent branch cuts in the $\zeta$-plane for the functions $a_{\pm} \equiv a_{\pm}(\zeta, p) = (m_{\pm}^2 - \zeta^2)^{1/2}$ and $\beta \equiv \beta(\zeta) = (m^2 - \zeta^2)^{1/2}$ as Fig. 2 depicts for the representative case of $\beta(\zeta)$ (i.e. outwards with respect to the origin $\zeta = 0$). In this way, $\mathrm{Re}(a_{\pm}, \beta) > 0$ in the cut plane. Also, in view of the definitions for $m_{\pm}$ and $m$, the following inequalities can be proven:

$$m_- < m_+ < m \quad \text{for } hp > \frac{m^2(1+\varepsilon) - 1}{m^2(m^2-1)}, \tag{20a}$$

$$m_- < m < m_+ \quad \text{for } hp < \frac{m^2(1+\varepsilon) - 1}{m^2(m^2-1)}, \tag{20b}$$

whereas Brock (1995) provides the following *approximate* forms which considerably simplify unilateral Laplace transform inversions:

$$m_+ \cong 1, \quad m_- \cong \frac{1}{(hp)^{1/2}} \quad \text{for } \frac{s}{h} \ll 1, \tag{21a}$$

$$m_+ \cong \left(\frac{1+\varepsilon}{hp}\right)^{1/2}, \quad m_- \cong \frac{1}{(1+\varepsilon)^{1/2}} \quad \text{for } \frac{s}{h} \gg 1. \tag{21b}$$

We notice that Eqs. (20a) and (20b) are necessary but not sufficient for the validity of Eqs. (21a) and (21b), respectively. Finally, it turns out that Eqs. (20a) and (21a) hold true only during a *very small* initial time-interval of the process which for most materials is $t < \mathrm{O}(10^{-14})$ s. In the present study, however, information is needed generally for longer times so we shall focus interest only on the case (20b) and employ Eq. (21b) appropriately. Since Eq. (21b) was obtained by considering $s \to (1/p)$ and expanding in series, any case $(s/h) \geqslant 100$ leads to a reasonable approximation for $m_{\pm}$.

Now, transforming via Eqs. (10a) and (11a) the continuity/discontinuity conditions (6a)–(6h) (with $g_Q(t) = g_P(t) = g_S(t) = g_R(t) = \delta(t)$) and the boundary conditions (7), in view also of the general transformed solutions (12) and (13), leads to a linear algebraic system of 12 equations in the 12 unknown

$X_1, X_2, \ldots, X_{12}$. Obviously, an exact (i.e. symbolical and not numerical) solution to the system is sought here and this was made possible by using MATHEMATICA™, version 3.0. The expressions for $X_1, X_2, \ldots, X_{12}$, which are quite lengthy in the general case of ($Q \neq 0$, $P \neq 0$, $S \neq 0$, $R \neq 0$), are not presented in this paper but can be found in the report by Lykotrafitis et al. (1999). Here, in Appendix B, the original system and the solution $(X_1, X_2, \ldots, X_{12})$ are given in the special case of ($Q \neq 0$, $P = S = R = 0$).

Having available the solution $(X_1, X_2, \ldots, X_{12})$ and therefore, by Eqs. (12) and (13), the general expressions for the double transformed temperature, displacements and stresses allows determining the field quantities at any point of the original space and at any time instant through successive *inversions* of the type (11b) and (10b). However, we emphasize at this point that a treatment employing the Cagniard–deHoop technique (Flinn and Dix, 1962; deHoop, 1960) to accomplish the transform inversions in an exact manner seems to be impossible due to the very complicated multiple transformed solution in the present problem. In simpler buried-source problems of non-thermal type such a difficulty was not met and the Cagniard–deHoop technique had successfully been applied (Pekeris, 1955; Garvin, 1956; Pekeris and Lifson, 1957; Aggarwal and Ablow, 1967; Payton, 1968, 1983; Johnson, 1974; Tsai and Ma, 1991). This is fully explained in Georgiadis et al. (1999a), so here it only suffices to note that in the thermal case, after the appropriate contour integration involved in the Cagniard–deHoop technique, the integrand in the semi-infinite branch-line integration is still $p$-dependent and, therefore, the unilateral transform inversion cannot be carried out through the standard inspection procedure. In the aforementioned work, nevertheless, an additional asymptotic argument eventually made possible the use of the Cagniard–deHoop technique but the results in that case were valid only for long time. In the present study, we take another way and rely exclusively on numerical analysis, by following the procedure of Georgiadis et al. (1999b), in order to accomplish the transform inversions. Below, details of the procedure and results will be given for the special but important case of a buried thermal source, i.e. for $Q \neq 0$ and $P = S = R = 0$, while we focus attention to the evaluation of the vertical displacement at the surface $u_z(x, y, z = -H, t)$.

Finally, notice that if a general dependence from time of the loading functions is to be considered (i.e. arbitrary $g_k(t)$, with $k = Q, P, S, R$, instead of $\delta(t)$), then the quantities $Q, P, S$ and $R$ in Eqs. (B.5)–(B.8) of Appendix B should be replaced by, respectively, $(Q/V_1)G_Q(p)$, $(P/V_1)G_P(p)$, $(S/V_1)G_S(p)$ and $(R/V_1)G_R(p)$, where $G_k(p)$ denote the unilateral Laplace transforms of the functions $g_k(s/V_1 \equiv t)$.

## 4. Further elaboration of the solution and preliminary results

In view of the previous results, the multiply transformed displacement $U_z^*(q, w, z = -H, p) \equiv U_z^*(\zeta, z = -H, p)$ for the case $Q \neq 0$ and $P = S = R = 0$ is given by

$$U_z^*(\zeta, z = -H, p) = \frac{\kappa Q V_1 T}{p^2} \frac{a_+ \mathrm{e}^{-a_- pH} - a_- \mathrm{e}^{-a_+ pH}}{D(\zeta, p)}, \tag{22}$$

where, as before, the complex variable $\zeta$ is defined through $\zeta^2 = q^2 + w^2$, and $a_\pm \equiv a_\pm(\zeta, p) = \left(m_\pm^2 - \zeta^2\right)^{1/2}$, $\beta \equiv \beta(\zeta) = \left(m^2 - \zeta^2\right)^{1/2}$ and $T = m^2 - 2\zeta^2$. We also define

$$D(\zeta, p) \equiv D = a_- M_- R_+ - a_+ M_+ R_-, \tag{23}$$

where the functions

$$R_+(\zeta, p) \equiv R_+ = 4\zeta^2 a_+ \beta + T^2, \qquad R_-(\zeta, p) \equiv R_- = 4\zeta^2 a_- \beta + T^2, \tag{24a, b}$$

can be identified as the *thermoelastic* counterparts of the non-thermal purely elastic transformed Rayleigh function, which is given as (Achenbach, 1973; Freund, 1990) $R_0 = 4\zeta^2 a\beta + T^2$, with $a \equiv a(\zeta) = (1 - \zeta^2)^{1/2}$. Contrary to the latter case, however, $R_\pm$ exhibit a $p$-dependence showing therefore that the thermoelastic Rayleigh waves in the physical space/time domain are *dispersive*. Another point to notice is that the very

definition of the variable $\zeta$ and the form of $U_z^*$ exhibit the axisymmetric nature of the problem with $Q \neq 0$ and $P = S = R = 0$, a fact which will become evident in the procedure that follows.

Finally, as in the plane-stress/strain case (Brock, 1995, 1997; Georgiadis et al. 1999a), by invoking the principle of the argument (Ablowitz and Fokas, 1997) it can be shown that the two real zeros $\zeta = \pm\zeta_R(p)$ of the function $(D/a_+)$ are the only zeros of this function in the entire $\zeta$-plane. These correspond to axisymmetric thermoelastic Rayleigh wavefronts propagating with a velocity $V_R(t) = V_1/\zeta_R$ along the traction-free half-space surface. Working with real $p$ such that $p > 0$ (which, of course, is necessary for the convergence of the integral defining the unilateral Laplace transform in Eq. (10a)) in the case of interest $m_- < m < m_+$ (cf. Eq. (20b)), we can obtain a closed-form expression for the root $\zeta_R$ by utilizing factorization operations (Noble, 1958; Roos, 1969; Ablowitz and Fokas, 1997) in the manner indicated by Brock (1995, 1997, 1998). The function $(D/a_+)$ is analytic in the $\zeta$-plane cut along $(m_- < |\mathrm{Re}(\zeta)| < m_+, \mathrm{Im}(\zeta) = 0)$ and behaves like $-2(m^2-1)\left(m_-^2 - m_+^2\right)\zeta^2$ as $|\zeta| \to \infty$. Consequently, the auxiliary function $S(\zeta, p)$ is introduced through the definition,

$$S \equiv \frac{(D/a_+)}{-2(m^2-1)\left(m_-^2 - m_+^2\right)\left(\zeta^2 - \zeta_R^2\right)}, \tag{25}$$

which possesses the desired asymptotic property $S(\zeta, p) \to 1$ as $|\zeta| \to \infty$ and, additionally, has neither zeros nor poles. The only singularities of $S$ are the branch points $\zeta = \pm m_-, \pm m_+$ which are shared with $(D/a_+)$, so it is single valued in the $\zeta$-plane cut along $(m_- < |\mathrm{Re}(\zeta)| < m_+, \mathrm{Im}(\zeta) = 0)$. Then, the standard technique of factorization through the use of Cauchy's integral theorem (Noble, 1958; Roos, 1969; Ablowitz and Fokas, 1997) allows writing

$$S = S^+ S^-, \tag{26}$$

where $S^+$ and $S^-$ are analytic functions in the overlapping half-planes $\mathrm{Re}(\zeta) > -m_-$ and $\mathrm{Re}(\zeta) < m_-$, respectively, and given as

$$S^{\pm}(\zeta, p) = \exp\left[\frac{1}{\pi}\int_{m_-}^{m} \arctan\left(\frac{|a_-|}{|a_+|}\left(\frac{M_-}{M_+} - |a_+|\frac{4\omega^2|\beta|}{T^2 B}\right)\right)\frac{\mathrm{d}\omega}{\omega \pm \zeta} + \frac{1}{\pi}\int_{m}^{m_+} \arctan\left(\frac{|a_-|}{|a_+|}\left(\frac{M_+}{M_-} + |a_-|\frac{4\omega^2|\beta|}{T^2 A}\right)^{-1}\right)\frac{\mathrm{d}\omega}{\omega \pm \zeta}\right], \tag{27}$$

where

$$A = -\frac{M_-}{M_+ - M_-}, \qquad B = \frac{M_+}{M_+ - M_-}. \tag{28a, b}$$

Further, one may observe from Eq. (27) that $S^+(\zeta = 0, p) = S^-(\zeta = 0, p)$ and, therefore, $S(\zeta = 0, p) = [S^+(\zeta = 0, p)]^2$. Now, by the latter result and Eqs. (25)–(27), it easily results the following explicit formula for the root of the function $(D/a_+)$:

$$\zeta_{\mathrm{R}}(p) = \frac{m^2[B + (m_-/m_+)A]^{1/2}}{[2(m^2-1)]^{1/2} S^+(\zeta = 0, p)}, \tag{29}$$

with the inequality $m < \zeta_{\mathrm{R}} < m_+$ always to hold. One final notice pertains to the variation of the thermoelastic Rayleigh-wave velocity with time. Indeed, in the study of Georgiadis, Brock and Rigatos (1998) it was shown that this velocity varies only slightly with time, a result explained in view of the fact that while there is a strong shear contribution (which remains unaffected by thermal effects) to the Rayleigh waves, the dilatational part of them is very weak (Viktorov, 1967).

The foregoing inspection on the behavior of the RHS of Eq. (22) will prove, certainly, to be advantageous in the inversion procedure that follows. In view of the definition (11b), one can write

$$U_z(x,y,z=-H,p)=\left(\frac{p}{2\pi i}\right)^2\int_{-i\infty}^{+i\infty}\int_{-i\infty}^{+i\infty}U_z^*(q,w,z=-H,p)\mathrm{e}^{pqx}\,\mathrm{e}^{pwy}\,\mathrm{d}q\,\mathrm{d}w, \tag{30}$$

where $U_z^*$ is given in Eq. (22). Next, axisymmetry (or radial symmetry) of the problem will become clear and be exploited. To this end, we set $q=\mathrm{i}\sigma$ and $w=\mathrm{i}\tau$ so that $\zeta^2\equiv q^2+w^2=-(\sigma^2+\tau^2)=-\rho^2$, and further consider the polar coordinates $(r,\theta)$ and $(\rho,\varphi)$ defined through the relations $x+\mathrm{i}y=r\mathrm{e}^{\mathrm{i}\theta}$ and $\sigma+\mathrm{i}\tau=\rho\mathrm{e}^{\mathrm{i}\varphi}$. The first set of polar coordinates refers to the physical plane $(x,y)$, whereas the second set to the transform plane $(\sigma,\tau)$. Considering also the case $x\geqslant 0$ and $y\geqslant 0$ (which, as will become clear soon, does not impose any restriction to the solution), it should be $\mathrm{Im}(\sigma)\geqslant 0$ and $\mathrm{Im}(\tau)\geqslant 0$, whereas $\rho\equiv(\sigma^2+\tau^2)^{1/2}\geqslant 0$. In view of Eqs. (22) and (30) and the latter considerations, one may obtain according to the relative procedure by Bracewell (1965):

$$U_z(r,\theta,z=-H,p)=\frac{\kappa QV_1}{4\pi^2}\int_0^{\infty}\int_0^{2\pi}\frac{a_+T\mathrm{e}^{-a_-Hp}-a_-T\mathrm{e}^{-a_+Hp}}{D(\rho,p)}\exp\left(\mathrm{i}pr\rho\cos(\varphi-\theta)\right)\mathrm{d}\varphi\rho\,\mathrm{d}\rho, \tag{31}$$

or

$$\begin{aligned}U_z(r,z=-H,p)&=\frac{\kappa QV_1}{4\pi^2}\int_0^{\infty}\frac{a_+T\mathrm{e}^{-a_-Hp}-a_-T\mathrm{e}^{-a_+Hp}}{D(\rho,p)}\left[\int_0^{2\pi}\exp(-\mathrm{i}pr\rho\cos\varphi)\,\mathrm{d}\varphi\right]\rho\,\mathrm{d}\rho\\&=\frac{\kappa QV_1}{2\pi}\int_0^{\infty}\frac{a_+T\mathrm{e}^{-a_-Hp}-a_-T\mathrm{e}^{-a_+Hp}}{D(\rho,p)}J_0(pr\rho)\rho\,\mathrm{d}\rho,\end{aligned} \tag{32}$$

where $a_{\pm}=\left(m_{\pm}^2+\rho^2\right)^{1/2}$, $\beta=(m^2+\rho^2)^{1/2}$, $T=m^2+2\rho^2$ and the following property of the Bessel function $J_0(\ )$ was used (Bracewell, 1965):

$$(1/2\pi)\int_0^{2\pi}\exp(-\mathrm{i}pr\rho\cos\varphi)\,\mathrm{d}\varphi=J_0(pr\rho), \tag{33}$$

whereas eliminating the variable $\theta$ from the problem is made possible by the observation that the inner integral in Eq. (31) is actually independent on the starting limit of the integration interval. Finally, another change of variable resulting from setting $\omega=pr\rho$ leads to the following expression for the unilateral Laplace transformed vertical displacement at the surface:

$$U_z(r,z=-H,p)=\frac{\kappa QV_1}{2\pi}\int_0^{\infty}\frac{(a_+\mathrm{e}^{-a_-Hp}-a_-\mathrm{e}^{-a_+Hp})T}{D(r,\omega,p)}\frac{\omega}{p^2r^2}J_0(\omega)\,\mathrm{d}\omega, \tag{34}$$

where the symbols $a_{\pm}$, $\beta$, $T$ take the following forms (which, of course, are compatible with the definitions (14) and (17a) and the several changes of variable in the previous analysis) and $D(r,\omega,p)$ is given in Eq. (23) with $\zeta^2$ being replaced by $-\omega^2/p^2r^2$:

$$a_{\pm}=\left(m_{\pm}^2+\frac{\omega^2}{p^2r^2}\right)^{1/2},\qquad \beta=\left(m^2+\frac{\omega^2}{p^2r^2}\right)^{1/2},\qquad T=m^2+2\frac{\omega^2}{p^2r^2}. \tag{35}$$

In this way, the double *complex* integration in Eq. (30) has been avoided since it was replaced by the single real integration in Eq. (34). Thus, before formally proceeding to the unilateral Laplace transform inversion we have to deal with the *wave number* integral in Eq. (34). However, the numerical procedure employed takes care of both operations in the same algorithm. This procedure will be presented in Section 5.

Closing this Section, the important limit case of $(r\to 0, H=0)$ is considered. The limit for the vertical surface displacement as the location of the *surface* source is approached can be obtained by the use of the

Abel-Tauber theorem (van der Pol and Bremmer, 1950; Roos, 1969). The displacement for $(r \to 0, H = 0)$ at $z = 0$ may result from the transformed displacement $U_z^*(\zeta, z = 0, H = 0, p)$ for $(|\zeta| \to \infty)$. Indeed, asymptotic considerations lead to the following expression:

$$\lim_{|\zeta|\to\infty} U_z^*(\zeta, z = 0, H = 0, p) = -\frac{\kappa Q V_1}{2(m^2-1)p^2}\frac{1}{\zeta^2}, \tag{36}$$

which when inverted according to Eqs. (34) and (10b) yields

$$\lim_{r\to 0} u_z(r, z = 0, H = 0, t) = \frac{\kappa Q}{4\pi(m^2-1)}\delta(t)\int_0^\infty \frac{J_0(\omega)}{\omega}\,\mathrm{d}\omega. \tag{37}$$

Now, the singular integral in Eq. (37) is found to behave like $[-\ln(\varepsilon/2)]$ with $\varepsilon \to +0$ (by 11.1.20 of Abramowitz and Stegun, 1982), so the displacement in question is logarithmically singular at the instant of application of the heat loading but becomes zero after removing it. This logarithmic singularity is compatible with the respective result of the uncoupled thermoelastostatic theory (Parkus, 1962).

## 5. Numerical procedure

The numerical procedure recently advanced for the classical Lamb's problem (Georgiadis et al. 1999b) is employed here. A brief presentation will only be given. First, the numerical unilateral Laplace-transform inversion is effected by using the Crump (1976) method (see also for related methods in Dubner and Abate (1968), Durbin (1976)). This method proved to be particularly successful as both survey articles (Davies and Martin, 1979; Narayanan and Beskos, 1982; Duffy, 1993) and previous experience (Georgiadis, 1993; Georgiadis and Rigatos, 1996) indicate. Of course, any numerical technique of this kind can provide reliable results only for a *bounded* time interval and not for the entire time domain because of the inevitable instability of the *first-kind* integral equation (10a) to a numerical treatment. Nevertheless, this boundedness requirement is not particularly restrictive if one is content to obtain results right after the application of the loading – which is the case in the present study – and is not interested in the long time solution. But even in the latter case, i.e. when a long time (or static) limit is sought, practically this limit occurs almost *immediately* after the arrival of the Rayleigh wavefront in two-dimensional (2D) plane stress/strain and 3D situations (see e.g. Freund, 1974, for the problem of a crack under concentrated loading, and Georgiadis et al. 1999b, for Lamb's point-load problem). Finally, it is noted that an alternative could be the spectral method of Geubelle and Rice (1995) which was also tested, with excellent results, against the analytical solution to Lamb's problem.

The starting point in the Crump (1976) method is the following alternative form of Eq. (10b)

$$\varphi(s) = \frac{\mathrm{e}^{\chi s}}{\pi}\int_0^\infty [\mathrm{Re}(\Phi(\chi + \mathrm{i}\psi))\cos(\psi s) - \mathrm{Im}(\Phi(\chi + \mathrm{i}\psi))\sin(\psi s)]\,\mathrm{d}\psi, \tag{38}$$

where $p = \chi + \mathrm{i}\psi$. In this way, the complex integral in Eq. (10b) is replaced by the real integral in Eq. (38), which offers the advantage of the application of a direct numerical scheme for its evaluation. Indeed, if the trapezoidal rule for semi-infinite integration intervals is applied to Eq. (38) (Davis and Rabinowitz, 1984), the following approximation of the *Fourier-series* type will result:

$$\varphi(s) \cong \left(\frac{\mathrm{e}^{\chi s}}{s_\mathrm{P}}\right)\left[\frac{\Phi(\chi)}{2} + \sum_{k=1}^{\infty}\left[\mathrm{Re}\left(\Phi\left(\chi + \frac{\mathrm{i}k\pi}{s_\mathrm{P}}\right)\right)\cos\left(\frac{k\pi s}{s_\mathrm{P}}\right) - \mathrm{Im}\left(\Phi\left(\chi + \frac{\mathrm{i}k\pi}{s_\mathrm{P}}\right)\right)\sin\left(\frac{k\pi s}{s_\mathrm{P}}\right)\right]\right]. \tag{39}$$

It is also noticed that Crump (1976) has presented a systematic error analysis from which $\varphi(s)$ can be computed to a predetermined accuracy. This means that the so-called period $s_\mathrm{P}$ and the abscissa $\chi$ should be

chosen according to this analysis (in fact, $s_P$ is taken so that $2s_P > s_{max}$, where $s_{max}$ is the normalized time up to which results are to be obtained, whereas the formula for $\chi$ is given below). In addition, the acceleration of the convergence of the summation in Eq. (39) is obtained by using the modified Epsilon algorithm introduced in Georgiadis et al. (1999b) (see for the original algorithm in MacDonald (1964) and Davis and Rabinowitz (1984). This means that only the first few terms of the series need to be calculated, and these are then utilized in a nonlinear combination to obtain very accurate results for the summation. One final notice pertains to the fact that $p$ in Crump's method is allowed to be complex, a situation offering (in a numerical Laplace-transform inversion) increased accuracy as compared with a treatment based on real $p$ (Crump, 1976; Davies and Martin, 1979). Translated into the present case, this means that we have first to consider the *analytic continuation* of our solution in Eq. (34) before its numerical inversion. This operation does not pose any difficulty, however, because it can be shown that all poles and branch points of the function in the integrand of Eq. (34) are situated along the imaginary axis of the complex $p$-plane. Therefore, the Bromwich inversion path $\Gamma_1$ in Eq. (10b) can be taken just slightly to the right of the line $\mathrm{Re}(p) = 0$ and, accordingly, this placement will enter through the constant $\chi_0$ in the following formula (Crump, 1976) determining the abscissa $\chi$ in Eqs. (38) and (39): $\chi = \chi_0 - [\ln(E)](2s_P)^{-1}$, where $E$ is the maximum allowable error. In our specific problem, the following choice of parameters was made $E = 10^{-8}$, $s_p = 0.8\ s_{max}$, $\chi_0 = 10^{-3}[\ln(E)](2s_P)^{-1}$ and 241 terms were introduced in the Epsilon algorithm.

Obviously, in order to evaluate $u_z(r, z = -H, s)$ through Eq. (39) for each $s$ one has first to evaluate $U_z(r, z = -H, (\chi + \mathrm{i}k\pi/s_P))$ through Eq. (34) for each $k$.

We proceed now to discuss the main cause of difficulty in numerically implementing Eq. (34). This is related to strong oscillatory behavior of the integrand due to both the Bessel function $J_0$ and the terms $\exp(-a_{\pm}Hp)$ (notice that $p$ is complex in the latter arguments). In numerically evaluating this integral, therefore, we resort to Longman's (1956) method according to which the zeros of the integrand are first evaluated, 'positive' and 'negative' areas are then computed through the Gauss 80-point rule, and finally the results of each separate integration are summed up with accelerated convergence provided by the modified epsilon algorithm. As compared to the case treated in Georgiadis et al. (1999b), the present situation is more complicated by the occurrence of additional zeros due to the terms $\exp(-a_{\pm}Hp)$. This situation can be better realized by observing the graphs of Figs. 3 and 4 obtained at a specific observation position $r$ and inverse time $p$. Indeed, we define the functions,

$$f(r, \omega, p, H) \equiv \frac{(a_+ \mathrm{e}^{-a_- Hp} - a_- \mathrm{e}^{-a_+ Hp})T}{D(r, \omega, p)} \frac{\omega}{p^2 r^2} J_0(\omega), \tag{40}$$

$$g(r, \omega, p, H) \equiv \frac{(a_+ \mathrm{e}^{-a_- Hp} - a_- \mathrm{e}^{-a_+ Hp})T}{D(r, \omega, p)} \frac{\omega}{p^2 r^2}, \tag{41}$$

and take the depth of the source $H = 100$ m and the following material constants: coupling coefficient $\varepsilon = 0.01$, thermoelastic characteristic length $h = 10^{-10}$ m, and Poisson's ratio $v = 0.20$ (a value which yields $m \equiv V_1/V_2 = 1.632993$ ). Then, Figs. 3 and 4 show, respectively, the variation of $\mathrm{Re}\, f$ and of both $\mathrm{Re}\, g$ and $\mathrm{Im}\, g$ with $\omega$ at $r = 100H$ and $p = 0.0002 + \mathrm{i}0.00654$. The graph in Fig. 4 permits also to identify the arrival of the various *wave fronts* at the observation point since interference with the Bessel function $J_0$ is avoided. This figure especially depicts the arrivals of the *dilatational* and *Rayleigh* wave (the *shear* wave arrives just before the Rayleigh) near $\omega = 60$ and 120, respectively. However, as the observation point moves closer to the epicenter, the results show pronounced effects due to the dilatational wave. On the contrary, effects due to the Rayleigh wave become more pronounced for distant observation positions. Finally, similar graphs show that at surface points near to the epicenter, terms $\exp(-a_{\pm}Hp)$ become dominant.

Other issues which merit attention are the following: (i) The peaks marking the arrival of each wave front occur at about the same value of $\omega$, although $r$ varies, since the normalization $\omega = pr\rho$ has been employed and the damping (due to thermoelasticity) is very small. (ii) The particular choice of the interval of the

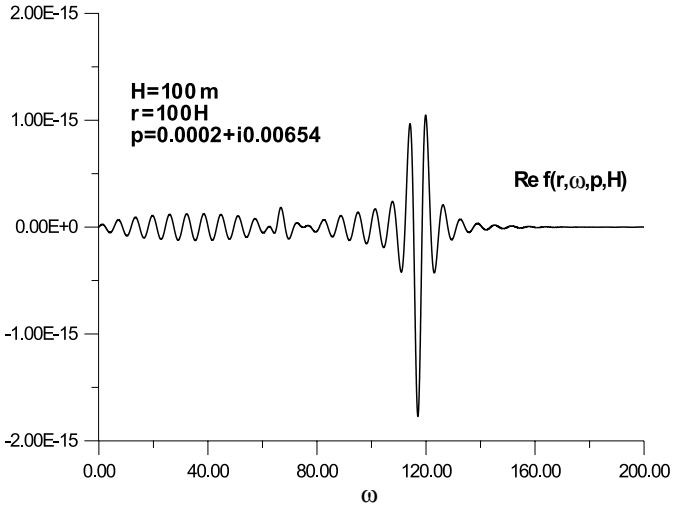


Fig. 3. Variation of Re$f$ with $\omega$ in the case $\varepsilon = 0.01$, $h = 10^{-10}$ m, $v = 0.20$, $H = 100$ m, $r = 100H$ and $p = 0.0002 + i0.00654$.

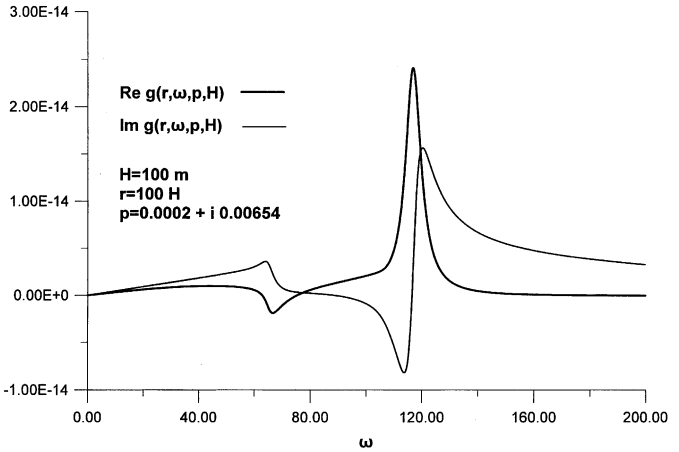


Fig. 4. Variation of Re$g$ and Im$g$ with $\omega$ in the case $\varepsilon = 0.01$, $h = 10^{-10}$ m, $v = 0.20$, $H = 100$ m, $r = 100H$ and $p = 0.0002 + i0.00654$.

normalized time in the graphs presenting our final results (for the variation of the vertical displacement at the surface) restricts the occurrence of peaks due to wave front arrivals up to the value $\omega = 300$. Accordingly, no accelerating technique is utilized within this interval and a careful treatment of these peaks is done in order to fully take into account the effects marking the wave front arrivals. The accelerating epsilon algorithm is utilized, however, after the value $\omega = 300$, i.e. in the interval where pure Bessel-function oscillations occur. (iii) Although the Rayleigh function $D(r, \omega, p)$ (which is complex-valued) is in the denominator of Eq. (34), the peaks associated with the thermoelastic Rayleigh wave are not of the type of a genuine Cauchy principal-value singularity because Re$D$ and Im$D$ do not vanish simultaneously for the same value of $\omega$ as long as the Bromwich path does not coincide with the Im$(p)$ axis. Indeed, this behavior of Re$D$ and Im$D$ can be observed in Fig. 5, where their variations with $\omega$ are presented for the case $H = 100$ m, $r = 100H$ and $p = 0.0002 + i0.00654$.

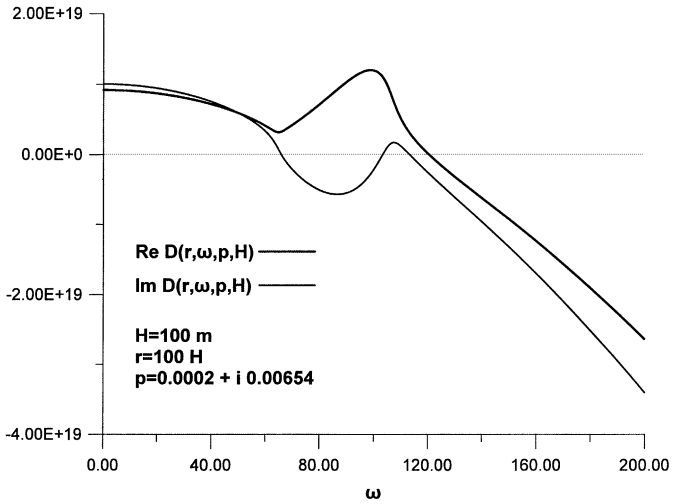


Fig. 5. Variation of $\mathrm{Re}\,D$ and $\mathrm{Im}\,D$ with $\omega$ in the case $\varepsilon = 0.01$, $h = 10^{-10}$ m, $v = 0.20$, $H = 100$ m, $r = 100H$ and $p = 0.0002 + \mathrm{i}0.00654$.

The existence of peaks (often resembling a pole-like behavior) in the functions $\mathrm{Re}\,f$ and $\mathrm{Im}\,f$ along with the oscillatory behavior requires a very careful integration scheme. The adaptive technique of Georgiadis et al. (1999b) is followed here but, as explained before, the present case is even more complicated. First, the roots of the functions $\mathrm{Re}\,g$ and $\mathrm{Im}\,g$ are found through the techniques of bracketing and bisection (Press et al., 1987), and also the zeros of the Bessel function $J_0$ are located (Table 9.5 of Abramowitz and Stegun (1982) was used for the first 20 points and of the McMahon formula – see e.g. Section 9.5 of the same source – for larger arguments). In this way, the zeros of the final functions $\mathrm{Re}\,f$ and $\mathrm{Im}\,f$ are obtained. Secondly, all local maxima and minima corresponding to wave front peaks are obtained in between consecutive zeros of $\mathrm{Re}\,f$ and $\mathrm{Im}\,f$. Finally, each integration interval between consecutive zeros is partitioned in the following two ways. If a wave front-related peak occurs in a particular interval, then 12 small sub-intervals are considered to the left and right of the peak abscissa and these become smaller and smaller as that point is approached (Georgiadis et al. 1999b). If, however, a rather smooth variation of the integrand occurs, then only four equal sub-intervals are considered. Throughout, the Longman (1965) procedure along with the Gauss 80-point rule was utilized. Also, no accelerating summation technique was used for the domain corresponding to the first 100 roots of $J_0$ (up to this point, all wave front-related peaks have already occurred), but the modified epsilon algorithm was then employed for the domain corresponding to the next 71 roots.

## 6. Numerical results and concluding remarks

The results we have obtained are given in the form of graphs showing the time variation (history) of the vertical displacement at the surface of the thermoelastic half-space. In these graphs, the normalized vertical displacement $u \equiv (2\pi u_z/\kappa Q V_1)$ and the normalized time $\tau \equiv [s/(r^2 + H^2)^{1/2}]$ are employed, whereas the following material constants were used: coupling coefficient $\varepsilon = 0.01$, thermoelastic characteristic length $h = 10^{-10}$ m, and Poisson's ratio $v = 0.20$. The graphs to be presented correspond to the case $H = 100$ m but a general result of our study is that the shape (profile) of the pulses remains essentially the same for the cases $H = 10$ and 1 m as long as normalization is utilized. Of course, the numerical values that the displacement takes on are different in each case (becoming larger for smaller depths).

The graphs in Figs. 6 and 7 show the history of the vertical displacement for $r = 40H$ and $r = 100H$, respectively, over the entire time domain considered in the inversion process. Generally, one could observe that, for distances near to the epicenter, the dilatational wave (arriving at the observation point at time $\tau \cong 1.0$) produces larger displacement than the shear and Rayleigh waves (the latter arriving at time $\tau \cong 1.7$) but, for distances far from the epicenter, the Rayleigh wave becomes the dominant one. Also, Fig. 8 depicts in more detail the profile of the dilatational wave by focusing to a small time interval near $\tau \cong 1.0$. The shape of this pulse reminds indeed the 'reversal' type of the pulses with the very steep variation observed in the study of Sternberg and Chakravorty (1959b), who pointed out the importance of *inertia* effects in thermal-shock problems and revealed, in fact, that such a 'reversal' effect at wave fronts is inherent to the

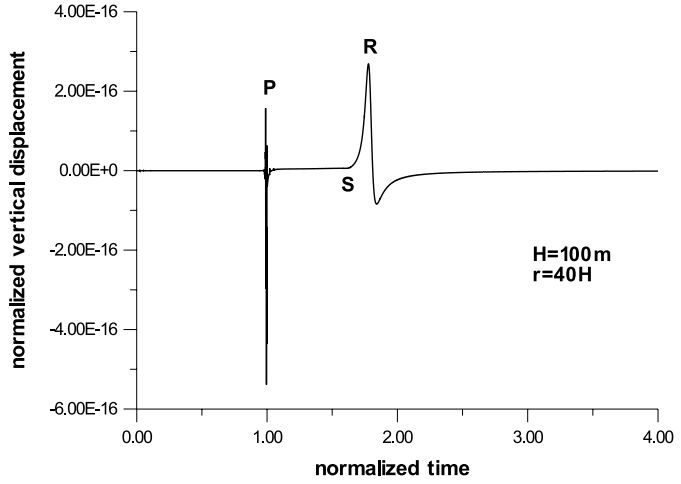


Fig. 6. Displacement $u$ vs. time $\tau$ graph in the case $\varepsilon = 0.01$, $h = 10^{-10}$ m, $v = 0.20$, $H = 100$ m and $r = 40H$. Arrivals of the dilatational (pressure), shear and Rayleigh waves are marked with the symbols P, S and R, respectively.

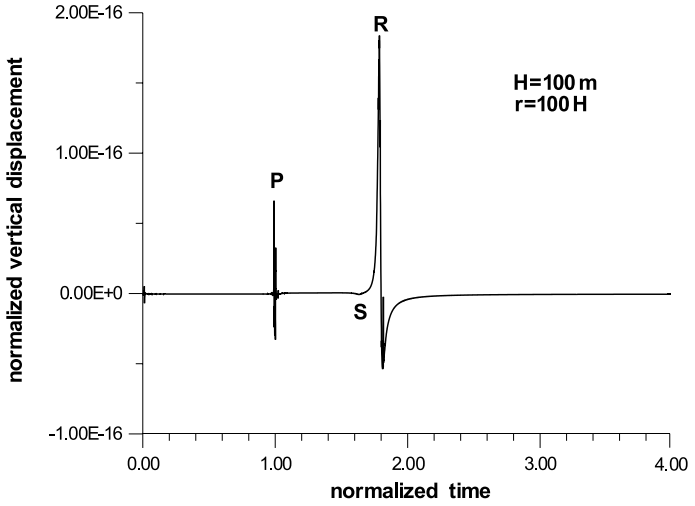


Fig. 7. Displacement $u$ vs. time $\tau$ graph in the case $\varepsilon = 0.01$, $h = 10^{-10}$ m, $v = 0.20$, $H = 100$ m and $r = 100H$. Arrivals of the dilatational (pressure), shear and Rayleigh waves are marked with the symbols P, S and R, respectively.

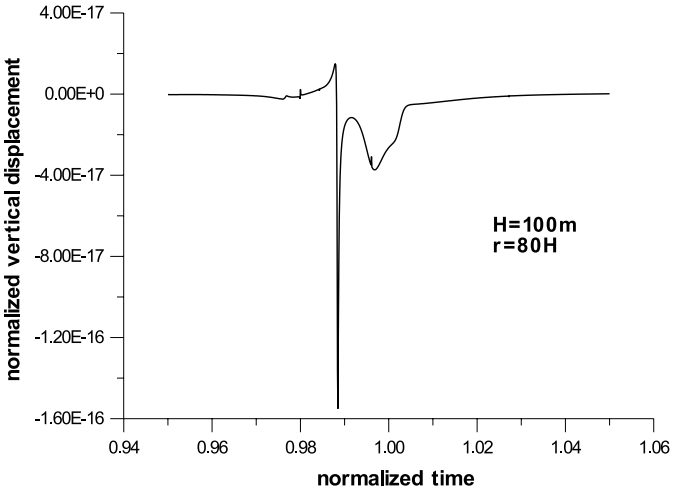


Fig. 8. Detail of the dilatational-wave profile in the case $\varepsilon = 0.01$, $h = 10^{-10}$ m, $v = 0.20$, $H = 100$ m and $r = 80H$.

*dynamical* theory of thermoelasticity. In fact, this type of pulses here indicates that precursor effects for the propagation of wave fronts are to be expected within Biot's thermoelasticity (see e.g. the relative discussion in Achenbach, 1973).

The next graphs, i.e. those in Figs. 9 and 10 (here, again, the case $H = 100$ m is considered), show in more detail the profiles of the shear and Rayleigh waves by considering times greater than the time of arrival of the dilatational wave. In this way, the stronger (especially at observation points close to the epicenter) dilatational disturbance does not overshadow the Rayleigh disturbance. These graphs indeed show the generation and initial development of the thermoelastic Rayleigh wave as the observation station moves away from the epicenter, but also show the decay in amplitude (attenuation due to the 3D geometry of the problem) after a certain point (see for analogous non-thermal situations in Pekeris and Lifson (1957) and Achenbach (1973)). The latter result is not encountered, certainly, in the respective 2-D problem (non-

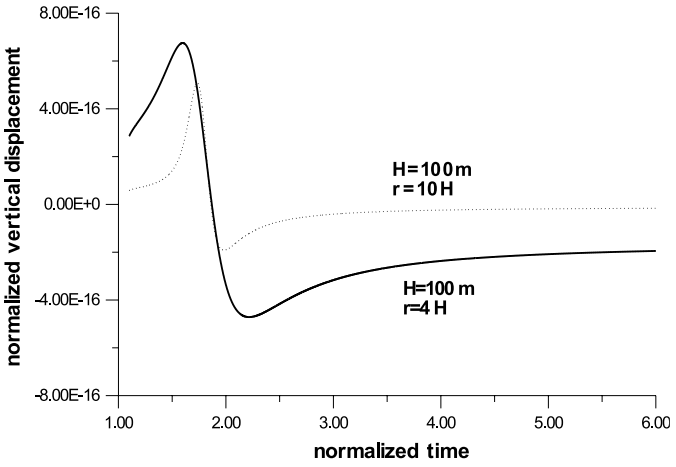


Fig. 9. Rayleigh-wave disturbances in the case $\varepsilon = 0.01$, $h = 10^{-10}$ m, $v = 0.20$, $H = 100$ m at two different observation stations $r = 4H$ and $10H$.

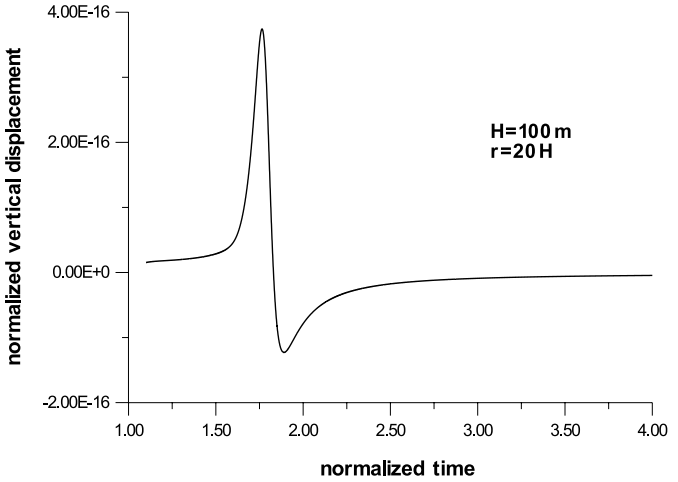


Fig. 10. Rayleigh-wave disturbance in the case $\varepsilon = 0.01$, $h = 10^{-10}$ m, $v = 0.20$, $H = 100$ m at the observation station $r = 20H$.

thermal buried dilatational source) of Garvin (1956) where once the Rayleigh pulse takes its shape, it is not decaying.

It is also of notice, in the two previous groups of graphs, that as the distance becomes greater the shape of each disturbance appears to become sharper because of the contraction of the real time scale with the increase of the length $(r^2 + H^2)^{1/2}$.

In conclusion, the 3D transient dynamic problem of a thermoelastic half-space under thermal and mechanical buried loads is treated in this paper. This problem is relevant to model both underground explosions and impulsively applied heat loadings near a boundary and, additionally, its solution provides the necessary Green's function needed in boundary element formulations of more complicated transient thermoelastodynamic problems. Biot's coupled thermoelasticity theory is considered and Laplace transforms along with symbolic algebra are utilized to get an exact solution in the multiple transform domain. From this solution, results for the vertical displacement at the surface due to a buried thermal source are obtained through numerical wave number integrations and numerical unilateral Laplace-transform inversions.

## Appendix A

Applying Eqs. (10a) and (11a) to the governing equations (1), (8), and (9), in view also of conditions (5), we obtain the following expressions for the transformed stresses:

$$\begin{aligned}
&\frac{1}{\mu}\Sigma^*_{xy} = pwU^*_x + pqU^*_y, \qquad \frac{1}{\mu}\Sigma^*_{xz} = D(U^*_x) + pqU^*_z, \qquad \frac{1}{\mu}\Sigma^*_{yz} = D(U^*_y) + pwU^*_z,\\
&\frac{1}{\mu}\Sigma^*_{xx} = \kappa\Theta^* + m^2pqU^*_x + \left(m^2-2\right)pwU^*_y + \left(m^2-2\right)D(U^*_z),\\
&\frac{1}{\mu}\Sigma^*_{yy} = \kappa\Theta^* + \left(m^2-2\right)pqU^*_x + m^2pwU^*_y + \left(m^2-2\right)D(U^*_z),\\
&\frac{1}{\mu}\Sigma^*_{zz} = \kappa\Theta^* + \left(m^2-2\right)pqU^*_x + \left(m^2-2\right)pwU^*_y + m^2D(U^*_z),
\end{aligned} \tag{A.1}$$

and the following system of linear ordinary differential equations for the transformed temperature change and displacements:

$$\begin{pmatrix} \frac{\kappa_v}{m^2}\left(p^2q^2+p^2w^2-\frac{p}{h}+D^2(\ )\right) & \frac{\varphi p^2 q}{h} & \frac{\varphi p^2 w}{h} & \frac{\varphi p}{h}D(\ ) \\ \kappa pq & [p^2w^2+p^2m^2(q^2-1)+D^2(\ )] & p^2q(m^2-1)w & pq(m^2-1)D(\ ) \\ \kappa pw & p^2qw(m^2-1) & [p^2q^2+p^2m^2(w^2-1)+D^2(\ )] & pw(m^2-1)D(\ ) \\ \kappa D(\ ) & pq(m^2-1)D(\ ) & pw(m^2-1)D(\ ) & [p^2(q^2+w^2-m^2)+m^2D^2(\ )] \end{pmatrix} \begin{pmatrix} \Theta^* \\ U_x^* \\ U_y^* \\ U_z^* \end{pmatrix} = 0, \tag{A.2}$$

where $D(\ )$ denotes the differential operator $\mathrm{d}(\ )/\mathrm{d}z$.

The determinant of the coefficient matrix has the simple roots $\pm pa_+$ and $\pm pa_-$, and also the double roots $p\beta$ and $-p\beta$. Accordingly, the general solution of Eq. (A.2) is found to be

$$\begin{aligned} \Theta^* &= a_1\mathrm{e}^{pa_+z}+a_2\mathrm{e}^{-pa_+z}+a_3\mathrm{e}^{pa_-z}+a_4\mathrm{e}^{-pa_-z}+a_5\mathrm{e}^{p\beta z}+a_6\mathrm{e}^{-p\beta z}, \\ U_x^* &= b_1\mathrm{e}^{pa_+z}+b_2\mathrm{e}^{-pa_+z}+b_3\mathrm{e}^{pa_-z}+b_4\mathrm{e}^{-pa_-z}+b_5\mathrm{e}^{p\beta z}+b_6\mathrm{e}^{-p\beta z}, \\ U_y^* &= c_1\mathrm{e}^{pa_+z}+c_2\mathrm{e}^{-pa_+z}+c_3\mathrm{e}^{pa_-z}+c_4\mathrm{e}^{-pa_-z}+c_5\mathrm{e}^{p\beta z}+c_6\mathrm{e}^{-p\beta z}, \\ U_z^* &= d_1\mathrm{e}^{pa_+z}+d_2\mathrm{e}^{-pa_+z}+d_3\mathrm{e}^{pa_-z}+d_4\mathrm{e}^{-pa_-z}+d_5\mathrm{e}^{p\beta z}+d_6\mathrm{e}^{-p\beta z}. \end{aligned} \tag{A.3}$$

Now, elimination of some of the coefficients, say $(a_j, c_j, d_j)$ with $(j = 1, 2, \ldots, 6)$, is obtained by a convenient substitution of Eq. (A.3) in Eq. (A.2). This substitution yields a system of three linear independent algebraic equations for each set $(a_k, b_k, c_k, d_k)$, with $(k = 1, 2, \ldots, 4)$, of the coefficients of the simple roots. Solving this system provides the coefficients $(a_k, c_k, d_k)$ as functions of $b_k$, with $(k = 1, 2, \ldots, 4)$. Finally, as regards the coefficients of the double-root terms, an additional linearly independent algebraic equation is provided by the first equation of the system (A.2).

Combining the results obtained through the above procedure gives the general solutions in Eqs. (12) and (13) of the main text.

## Appendix B

The $12 \times 12$ system of Section 3 reads

$$X_1 + X_2 - \frac{1}{q}X_3 - X_5 - X_6 - X_7 - X_8 + \frac{1}{q}X_9 + \frac{1}{q}X_{11} = 0, \tag{B.1}$$

$$X_1 + X_2 - \frac{1}{w}X_4 - X_5 - X_6 - X_7 - X_8 + \frac{1}{w}X_{10} + \frac{1}{w}X_{12} = 0, \tag{B.2}$$

$$X_1 + \frac{a_-}{a_+}X_2 + \frac{q}{\beta a_+}X_3 + \frac{w}{\beta a_+}X_4 + X_5 - X_6 + \frac{a_-}{a_+}X_7 - \frac{a_-}{a_+}X_8 + \frac{q}{\beta a_+}X_9 + \frac{w}{\beta a_+}X_{10} - \frac{q}{\beta a_+}X_{11} - \frac{w}{\beta a_+}X_{12} = 0, \tag{B.3}$$

$$X_1 + \frac{M_-}{M_+}X_2 - X_5 - X_6 - \frac{M_-}{M_+}X_7 - \frac{M_-}{M_+}X_8 = 0, \tag{B.4}$$

$$X_1 + X_2 + \frac{2q}{T}X_3 + \frac{2w}{T}X_4 - X_5 - X_6 - X_7 - X_8 - \frac{2q}{T}X_9 - \frac{2w}{T}X_{10} - \frac{2q}{T}X_{11} - \frac{2w}{T}X_{12} = -\frac{PV_1}{\mu T}, \tag{B.5}$$

$$X_1+\frac{a_-}{a_+}X_2-\frac{T_w}{2qa_+\beta}X_3+\frac{w}{2a_+\beta}X_4+X_5-X_6+\frac{a_-}{a_+}X_7-\frac{a_-}{a_+}X_8-\frac{T_w}{2qa_+\beta}X_9+\frac{w}{2a_+\beta}X_{10}+\frac{T_w}{2qa_+\beta}X_{11}-\frac{w}{2a_+\beta}X_{12}=\frac{SV_1}{2\mu qa_+},\tag{B.6}$$

$$X_1+\frac{a_-}{a_+}X_2+\frac{q}{2a_+\beta}X_3-\frac{T_q}{2wa_+\beta}X_4+X_5-X_6+\frac{a_-}{a_+}X_7-\frac{a_-}{a_+}X_8+\frac{q}{2a_+\beta}X_9-\frac{T_q}{2wa_+\beta}X_{10}-\frac{q}{2a_+\beta}X_{11}+\frac{T_q}{2wa_+\beta}X_{12}=\frac{RV_1}{2\mu wa_+},\tag{B.7}$$

$$X_1+\frac{M_-a_-}{M_+a_+}X_2+X_5-X_6+\frac{M_-a_-}{M_+a_+}X_7-\frac{M_-a_-}{M_+a_+}X_8=\frac{-QV_1\kappa}{M_+pa_+m^2},\tag{B.8}$$

$$\left(T\mathrm{e}^{-pa_+H}\right)X_5+\left(T\mathrm{e}^{pa_+H}\right)X_6+\left(T\mathrm{e}^{-pa_-H}\right)X_7+\left(T\mathrm{e}^{pa_-H}\right)X_8+\left(2q\mathrm{e}^{-p\beta H}\right)X_9+\left(2w\mathrm{e}^{-p\beta H}\right)X_{10}+\left(2q\mathrm{e}^{p\beta H}\right)X_{11}+\left(2w\mathrm{e}^{p\beta H}\right)X_{12}=0,\tag{B.9}$$

$$\left(-2qa_+\mathrm{e}^{-pa_+H}\right)X_5+\left(2qa_+\mathrm{e}^{pa_+H}\right)X_6+\left(-2qa_-\mathrm{e}^{-pa_-H}\right)X_7+\left(2qa_-\mathrm{e}^{pa_-H}\right)X_8+\left(\frac{T_w}{\beta}\mathrm{e}^{-p\beta H}\right)X_9+\left(-\frac{wq}{\beta}\mathrm{e}^{-p\beta H}\right)X_{10}+\left(-\frac{T_w}{\beta}\mathrm{e}^{p\beta H}\right)X_{11}+\left(\frac{wq}{\beta}e^{p\beta H}\right)X_{12}=0,\tag{B.10}$$

$$\left(-2wa_+\mathrm{e}^{-pa_+H}\right)X_5+\left(2wa_+\mathrm{e}^{pa_+H}\right)X_6+\left(-2wa_-\mathrm{e}^{-pa_-H}\right)X_7+\left(2wa_-\mathrm{e}^{pa_-H}\right)X_8+\left(-\frac{wq}{\beta}\mathrm{e}^{-p\beta H}\right)X_9+\left(\frac{T_q}{\beta}\mathrm{e}^{-p\beta H}\right)X_{10}+\left(\frac{wq}{\beta}\mathrm{e}^{+p\beta H}\right)X_{11}+\left(-\frac{T_q}{\beta}\mathrm{e}^{p\beta H}\right)X_{12}=0,\tag{B.11}$$

$$\left(M_+pa_+\mathrm{e}^{-pa_+H}\right)X_5-\left(M_+pa_+\mathrm{e}^{pa_+H}\right)X_6+\left(M_-pa_-\mathrm{e}^{-pa_-H}\right)X_7-\left(M_-pa_-\mathrm{e}^{pa_-H}\right)X_8=0,\tag{B.12}$$

and its solution in the specific case of $(Q\neq 0, P=S=R=0)$ is given by

$$X_1=-\kappa QV_1\mathrm{e}^{-2a_-Hp}\left[-\left(\mathrm{e}^{2a_-Hp}-\mathrm{e}^{-2(a_+-a_-)Hp}\right)a_-M_-TE+\left(\mathrm{e}^{2a_-Hp}+\mathrm{e}^{-2(a_+-a_-)Hp}-2\frac{M_-}{M_+}\mathrm{e}^{-(a_+-a_-)Hp}\right)a_+M_+TE+\left(\mathrm{e}^{2a_-Hp}+\mathrm{e}^{-2(a_+-a_-)Hp}\right)D\right]\Big/(BA),\tag{B.13}$$

$$X_2=\kappa QV_1\left\{-a_-\mathrm{e}^{-(a_++3a_-)Hp}\left[-2\mathrm{e}^{2a_-Hp}+\left(\mathrm{e}^{(a_++a_-)Hp}+\mathrm{e}^{(a_++3a_-)Hp}\right)\frac{M_-}{M_+}\right]M_+TE+\mathrm{e}^{-2a_-Hp}\times\left[\left(-1+\mathrm{e}^{2a_-Hp}\right)M_+a_+TE+\left(1+\mathrm{e}^{2a_-Hp}\right)D\right]\right\}\Big/(AC),\tag{B.14}$$

$$X_3=-2\kappa QV_1\beta qT\mathrm{e}^{-(a_++a_-+\beta)Hp}\left(a_+\mathrm{e}^{a_+Hp}-a_-\mathrm{e}^{a_-Hp}\right)\left(T_q+w^2\right)/(FA),\tag{B.15}$$

$$X_4=2\kappa QV_1\beta wT\mathrm{e}^{-(a_++a_-+\beta)Hp}\left(a_+\mathrm{e}^{a_+Hp}-a_-\mathrm{e}^{a_-Hp}\right)\left(T_w+q^2\right)/(FA),\tag{B.16}$$

$$X_5=-\frac{\kappa QV_1}{2a_+m^2p(M_+-M_-)}=-\frac{\kappa QV_1}{B},\tag{B.17}$$

$$X_6 = -\kappa Q V_1 \mathrm{e}^{-(2a_+ + a_-)Hp}\left\{a_- \mathrm{e}^{a_- Hp} M_- TE + a_+\left[\left(\mathrm{e}^{a_- Hp} M_+ - 2\mathrm{e}^{a_+ Hp} M_-\right)TE\right] + \mathrm{e}^{a_- Hp} D/(BA)\right\}, \tag{B.18}$$

$$X_7 = \frac{\kappa Q V_1}{C}, \tag{B.19}$$

$$X_8 = \kappa Q V_1 \mathrm{e}^{-(a_+ + 2a_-)Hp}\left[a_-\left(2\mathrm{e}^{a_- Hp} M_+ - \mathrm{e}^{a_+ Hp} M_-\right)TE + a_+ \mathrm{e}^{a_+ Hp}[M_+ T(-E)] + \mathrm{e}^{a_+ Hp} D\right]/(CA), \tag{B.20}$$

$$X_9 = X_{10} = 0, \tag{B.21}$$

$$X_{11} = -2\kappa Q V_1 \beta q T \mathrm{e}^{-(a_+ + \beta)Hp}\left(-a_- + a_+ \mathrm{e}^{(a_+ - a_-)Hp}\right)\left(T_q + w^2\right)/(FA), \tag{B.22}$$

$$X_{12} = 2\kappa Q V_1 \beta w T \mathrm{e}^{-(a_+ + a_- + \beta)Hp}\left(-a_+ \mathrm{e}^{a_+ Hp} + a_- \mathrm{e}^{a_- Hp}\right)\left(T_w + q^2\right)/(FA), \tag{B.23}$$

where

$$A = (a_+ M_+ - a_- M_-)T\left(T_q T_w - q^2 w^2\right) + 4a_+ a_- \beta (M_+ - M_-)\left(q^2 T_q + 2q^2 w^2 + w^2 T_w\right), \tag{B.24}$$

$$B = 2a_+ m^2 (M_+ - M_-)p, \tag{B.25}$$

$$C = 2a_- m^2 (M_+ - M_-)p, \tag{B.26}$$

$$D = 4a_+ a_- \beta (M_+ - M_-)\left(q^2 T_q + 2q^2 w^2 + w^2 T_w\right), \tag{B.27}$$

$$E = T_q T_w - q^2 w^2, \tag{B.28}$$

$$F = m^2 p. \tag{B.29}$$

## References


Ablowitz, M.J., Fokas, A.S., 1997. Complex Variables: Introduction and Applications. Cambridge University Press, Cambridge, MA.

Abramowitz, M., Stegun, I.A., 1982. Handbook of Mathematical Functions. Dover, New York.

Achenbach, J.D., 1973. Wave Propagation in Elastic Solids. North-Holland, New York.

Aggarwal, H.R., Ablow, C.M., 1967. Solution to a class of three-dimensional pulse propagation problems in an elastic half-space. Int. J. Engng. Sci. 5, 663–679.

Atkinson, C., Craster, R.V., 1992. Fracture in fully coupled dynamic thermoelasticity. J. Mech. Phys. Solids 40, 1415–1432.

Bechtel, J.H., 1975. Heating of solid targets with laser pulses. J. Appl. Phys. 46, 1585–1593.

Biot, M.A., 1956. Thermoelasticity and irreversible thermodynamics. J. Appl. Phys. 27, 240–253.

Boley, B.A., Tolins, I.S., 1962. Transient coupled thermoelastic boundary value problems in the half-space. ASME J. Appl. Mech. 29, 637–646.

Bracewell, R., 1965. The Fourier Transform and Its Applications. McGraw-Hill, New York.

Brock, L.M., 1995. Slip/diffusion zone formation at rapidly-loaded cracks in thermoelastic solids. J. Elasticity 40, 183–206.

Brock, L.M., 1997. Transient three-dimensional Rayleigh and Stoneley signal effects in thermoelastic solids. Int. J. Solids Struct. 34, 1463–1478.

Brock, L.M., 1998. Analytic results for roots of two irrational functions in elastic wave propagation. J. Austral. Math. Soc. Ser. B 40, 72–79.

Brock, L.M., Rodgers, M., Georgiadis, H.G., 1996. Dynamic thermoelastic effects for half-planes and half-spaces with nearly-planar surfaces. J. Elasticity 44, 229–254.

Brock, L.M., Georgiadis, H.G., Tsamasphyros, G., 1997. The coupled thermoelasticity problem of the transient motion of a line heat/mechanical source over a half-space. J. Thermal Stresses 20, 773–795.

Bullen, K.E., Bolt, B.A., 1987. An Introduction to the Theory of Seismology. Cambridge University Press, Cambridge, MA.

Burridge, R., Knopoff, L., 1964. Body force equivalents for seismic dislocations. Bull. Seismological Soc. Am. 54, 1875–1888.

Carlson, D.E., 1972. Linear Thermoelasticity. In: Flugge, S. (Ed.), Handbuch der Physik, vol. VIa/2. Springer, Berlin, pp. 297–345.
Chadwick, P., 1960. Thermoelasticity: The dynamical theory. In: Sneddon, I.N., Hill, R. (Eds.), Progress in Solid Mechanics, vol. 1. North-Holland, Amsterdam, pp. 263–328.
Chen, C.K., Kuo, B.L., 1994. Coupled transient thermoelastic contact problem in an edge-cracked plate. ASME J. Appl. Mech. 61, 736–738.
Crump, K.S., 1976. Numerical inversion of Laplace transforms using a Fourier series approximation. J. Assoc. Comp. Mach. 23, 89–96.
Davies, B., Martin, B., 1979. Numerical inversion of the Laplace transform: a survey and comparison of methods. J. Comp. Phys. 33, 1–32.
Davis, P.J., Rabinowitz, P., 1984. Methods of Numerical Integration, Academic Press, New York.
deHoop, A.T., 1960. The surface line source problem. Appl. Sci. Res. B 8, 349–356.
Dubner, H., Abate, J., 1968. Numerical inversion of Laplace transforms by relating them to the finite Fourier cosine transform. J. Assoc. Comp. Mach. 15, 115–123.
Duffy, D.G., 1993. On the numerical inversion of Laplace transforms: comparison of three new methods on characteristic problems from applications. ACM Trans. Math. Software 19, 333–359.
Durbin, F., 1976. Numerical inversion of Laplace transforms: an efficient improvement to Dubner and Abate's method. Comp. J. 17, 371–376.
Fleurier, J., Predeleanu, M., 1987. On the use of coupled fundamental solutions in B.E.M. for thermoelastic problems. Engng. Anal. 4, 70–74.
Flinn, E.A., Dix, C.H., 1962. Reflection and Refraction of Progressive Seismic Waves. McGraw-Hill, Berlin (Cagniard, L., 1939. Trans.; Reflexion et Refraction des Ondes Seismiques Progressive. Gauthier-Villard, Paris).
Francis, P.H., 1972. Thermo-mechanical effects in elastic wave propagation: a survey. J. Sound Vibrat. 21, 181–192.
Freund, L.B., 1974. The stress intensity factor due to normal impact loading of the faces of a crack. Int. J. Engng. Sci. 12, 179–189.
Freund, L.B., 1990. Dynamic Fracture Mechanics, Cambridge University Press, Cambridge, MA.
Garvin, W.W., 1956. Exact transient solution of the buried line source problem. Proc. Royal Soc. Lond. A234, 528–541.
Georgiadis, H.G., 1993. Shear and torsional impact of cracked viscoelastic bodies – A numerical integral equation/transform approach. Int. J. Solids Struct. 30, 1891–1906.
Georgiadis, H.G., Rigatos, A.P., 1996. Transient SIF results for a cracked viscoelastic strip under concentrated impact loading – an integral-transform/function-theoretic approach. Wave Motion 24, 41–57.
Georgiadis, H.G., Brock, L.M., Rigatos, A.P., 1998. Transient concentrated thermal/mechanical loading of the faces of a crack in a coupled-thermoelastic solid. Int. J. Solids Struct. 35, 1075–1097.
Georgiadis, H.G., Rigatos, A.P., Brock, L.M., 1999a. Thermoelastodynamic disturbances in a half-space under the action of a buried thermal/mechanical line source. Int. J. Solids Struct. 36, 3639–3660.
Georgiadis, H.G., Vamvatsikos, D., Vardoulakis, I., 1999b. Numerical implementation of the integral-transform solution to Lamb's point-load problem. Comput. Mech. 24, 90–99.
Geubelle, P.H., Rice, J.R., 1995. A spectral method for three-dimensional elastodynamic fracture problems. J. Mech. Phys. Solids 43, 1791–1824.
Hata, T., 1995. The determination of stress focusing intensity factor due to a spherical thermal inclusion in a sphere. In: Noda, N., Hetnarski, R. (Eds.), Proc. Int. Conf. Thermal Stresses-95, pp. 155–158.
Hegemier, G.A., Tzung, F., 1970. Stress-wave generation in a temperature-dependent absorbing solid by impulsive electromagnetic radiation. ASME J. Appl. Mech. 37, 339–344.
Hetnarski, R.B., 1961. Coupled one-dimensional thermal shock problem for small times. Arch. Mech. Stos. 13, 295–306.
Hetnarski, R.B., Ignaczak, J., 1994. Generalized thermoelasticity: response of semi-space to a short laser pulse. J. Thermal Stresses 17, 377–396.
Johnson, L.R., 1974. Green's functions for Lamb's problem. Geophys. J. R. Astr. Soc. 37, 99–131.
Ignaczak, J., Nowacki, W., 1962. The Sommerfeld radiation conditions for coupled problems of thermoelasticity. Examples of coupled stress and temperature concentration at cylindrical and spherical cavities. Archiwum Mechaniki Stosowanej 1, 3–13.
Lih, S., Mal, A.K., 1992. Elastodynamic response of a unidirectional composite laminate to concentrated surface loads: part I. ASME J. Appl. Mech. 59, 887–892.
Longman, I.M., 1956. Note on a method for computing infinite integrals of oscillatory functions. Proc. Camb. Phil. Soc. 52, 764–768.
Lykotrafitis, G., Georgiadis, H.G., Brock, L.M., 1999. Three-dimensional thermoelastic wave motions in a half-space under the action of a buried source. Mechanics Division Report, Natl. Tech. Univ. Athens, September.
MacDonald, J.R., 1964. Accelerated convergence, divergence, iteration, extrapolation and curve fitting. J. Appl. Phys. 35, 3034–3041.
Mal, A.K., Lih, S., 1992. Elastodynamic response of a unidirectional composite laminate to concentrated surface loads: part I. ASME J. Appl. Mech. 59, 878–885.
Manolis, G.D., Beskos, D.E., 1989. Integral formulation and fundamental solutions of dynamic poroelasticity and thermoelasticity. Acta Mech. 76, 89–104.

Manolis, G.D., Beskos, D.E., 1990. Integral formulation and fundamental solutions of dynamic poroelasticity and thermoelasticity. Acta Mech. 83, 223–226.
Morland, L.W., 1968. Generation of thermoelastic stress waves by impulsive electromagnetic radiation. AIAA J. 6, 1063–1070.
Narayanan, G.V., Beskos, D.E., 1982. Numerical operational methods for time-dependent linear problems. Int. J. Num. Meth. Engng. 18, 1829–1854.
Noble, B., 1958. Methods Based on the Wiener-Hopf Technique. Pergamon Press, New York.
Parkus, H., 1962. Thermal stresses. In: Flugge, W. (Ed.), Handbook of Engineering Mechanics. McGraw-Hill, New York, pp. 1–20 (Chapter 43).
Payton, R.G., 1968. Epicenter motion of an elastic half-space due to buried stationary and moving line sources. Int. J. Solids Struct. 4, 287–300.
Payton, R.G., 1983. Elastic Wave Propagation in Transversely Isotropic Media. Martinus Nijhoff, The Hague.
Pekeris, C.L., 1955. The seismic buried pulse. Proc. Natl. Acad. Sci. 41, 629–638.
Pekeris, C.L., Lifson, H., 1957. Motion of the surface of a uniform elastic half-space produced by a buried pulse. J. Acoust. Soc. Am. 29, 1233–1238.
Predeleanu, M., 1987. Analysis of thermomechanical coupling by boundary element method. In: Bui, H.D., Nguyen, Q.S. (Eds.), Thermomechanical Couplings in Solids. Elsevier, Amsterdam, pp. 305–318.
Press, W.H., Flannery, B.P., Teukolsky, S.A., Vetterling, W.T., 1987. Numerical Recipes: The Art of Scientific Computing. Cambridge University Press, Cambridge, MA.
Roos, B.W., 1969. Analytic Functions and Distributions in Physics and Engineering. Wiley, New York.
Sharp, S., Crouch, S.L., 1987. Heat conduction, thermoelasticity and consolidation. In: Beskos, D.E. (Ed.), Boundary Element Methods in Mechanics, Elsevier, Amsterdam, pp. 440–498.
Sternberg, E., Chakravorty, J.G., 1959a. On inertia effects in a transient thermoelastic problem. ASME J. Appl. Mech. 26, 503–509.
Sternberg, E., Chakravorty, J.G., 1959b. Thermal shock in an elastic body with a spherical cavity. Quart. Appl. Math. 17, 205–218.
Sve, C., Miklowitz, J., 1973. Thermally induced stress waves in an elastic layer. ASME J. Appl. Mech. 40, 161–168.
Tsai, C.H., Ma, C.C., 1991. Exact transient solutions of buried dynamic point forces and displacement jumps for an elastic half space. Int. J. Solids Struct. 28, 955–974.
van der Pol, B., Bremmer, H., 1950. Operational Calculus Based on the Two-Sided Laplace Integral. Cambridge University Press, Cambridge, MA.
Vardoulakis, I., Harnpattanapanich, T., 1986. Numerical Laplace-Fourier transform inversion technique for layered-soil consolidation problems: I Fundamental solutions and validation. Int. J. Num. Anal. Meth. Geomech. 10, 347–366.
Viktorov, I.A., 1967. Rayleigh and Lamb Waves. Plenum Press, New York.
Wang, J., Dhaliwal, R.S., 1993. Fundamental solutions of the generalized thermoelastic equations. J. Thermal Stresses 16, 135–161.
Xu, P., Mal, A.K., 1985. An adaptive integration scheme for irregularly oscillatory functions. Wave Motion 7, 235–243.